SEE Testing in the 24-GeV Proton Beam at the CHARM Facility

Rubén García Alía, Markus Brugger, Matteo Cecchetto, Francesco Cerutti, Salvatore Danzeca, Marc Delrieux, Maria Kastriotou, Maris Tali, and Slawosz Uznanski

***Abstract*— A 24-GeV proton beam is available at the Cern High energy AcceleRator Mixed field facility which can be used to test components and boards for single-event effects (SEEs) at a worst case energy for both accelerator and interplanetary space applications. The main beam characteristics are described, and SEE results for three different components are presented in combination with Monte Carlo results, focusing on the significant energy dependence, and risk of underestimating the operational error rate for hard spectral environments when considering SEE cross sections measured at proton cyclotron facilities.**

***Index Terms*— Cern High energy AcceleRator Mixed field facility (CHARM), European Space Agency (ESA) monitor, FLUKA, high-Z, nuclear reactions, single event upset (SEU), worst case energy.**

I. Introduction

A 24-GeV proton beam is available in the Cern High energy AcceleRator Mixed field facility (CHARM) at the European Centre for Nuclear Research (CERN). The beam is extracted from the proton synchrotron (PS) accelerator, one of the large hadron collider (LHC) injectors, to the T8 beam line in the experimental East Area (EA). During its standard operation, a mixed field environment is produced at CHARM through the interaction of the 24-GeV proton beam on a 50-cm metallic target in order to reproduce a radiation field similar to that present in the LHC accelerator and its surroundings [1]. However, it is also possible to remove the target and tune the beam optics in order to obtain a suitable beam for radiation effects testing directly with 24-GeV protons. The beam size and energy allow for testing of various components and boards in parallel.

Standards for qualifying components against single-event effects (SEEs) in the space and terrestrial environment using monoenergetic proton beams define 200 MeV as the maximum experimental energy value. For instance, the European Space Components Coordination (ESCC) SEEs test methods and guidelines (ESCC 25 100) recommends testing for protons in the 20–200 MeV range for space applications. Similarly, the JESD89A Joint Electron Device Engineering Council (JEDEC) standard [2] for terrestrial cosmic ray induced soft errors recommends using 14-MeV neutrons and protons of energies of approximately 50, 100, and 200 MeV. The retrieved cross sections as a function of energy can then be folded with the operational proton or neutron spectrum in order to retrieve the estimated SEE rate.

The definition of 200 MeV as maximum test energy is partially motivated by the fact that: 1) only a small fraction of the operational hadronic spectra remain above this energy and 2) the nuclear reaction cross section and linear energy transfer (LET) distribution of the recoils and fragments from nuclear interactions in silicon very weakly depend on the energy above this value [3], [4]. This upper energy limit is also practical due to the reasonably large availability of medical cyclotrons capable of producing it. However, as initially shown in [5], the presence of high-Z materials such as tungsten near the sensitive SEE areas can introduce a strong SEE cross section dependence with energy; therefore it is recommended to qualify components at the largest proton energy present in the operational environment. As will be shown in Section II, this can be a challenging constraint for environments with harder spectra than those present in the trapped proton belts.

This paper is structured as follows. A variety of radiation environments will be presented in Section II focusing in the hadron energy spectra with respect to the maximum energy defined in the standards. In Section III, we introduce the Monte Carlo model used to calculate the SEE cross section for a large variety of particles and energies. Section IV defines the beam characteristics at CHARM. Section V reports the measured single event upset (SEU) cross section at 24 GeV for two static random access memory (SRAM) memories and an analog-to-digital converter (ADC) with very different responses as a function of energy. Section VI summarizes the state-of-the-art with respect to the impact of high-Z material on qualification approaches and introduces a simplified SEE model with the purpose of extracting the relevant radiation hardness assurance (RHA) implications, which are discussed in Section VII. Finally, Section VIII summarizes the results and provides an outlook to the future related work.

II. Environmental Spectral Hardness

In order to scrutinize the spectral hardness of different radiation environments relevant to the operation of electronics, various particle differential energy spectra are compared in Fig. 1. All hadrons are considered together, as they can, in first approximation, be regarded as equally efficient in inducing SEEs due to their similar nuclear interaction cross sections [6]. The trapped proton spectrum corresponds to a

Manuscript received January 17, 2018; revised March 2, 2018 and March 7, 2018; accepted March 11, 2018. Date of publication April 25, 2018; date of current version August 15, 2018.

The authors are with CERN, CH-1211 Genève, Switzerland (e-mail: ruben.garcia.alia@cern.ch).

Color versions of one or more of the figures in this paper are available online at http://ieeexplore.ieee.org.

Digital Object Identifier 10.1109/TNS.2018.2829916

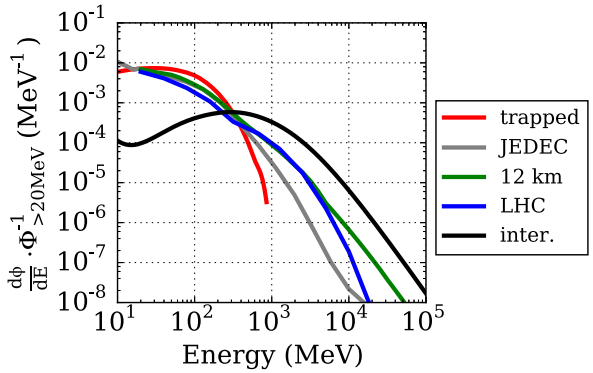

Fig. 1. Hadron differential energy spectra for various environments normalized to the integrated flux above 20 MeV.

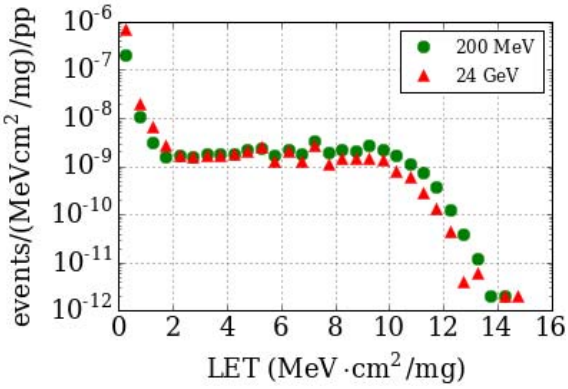

Fig. 2. Nuclear reaction product LET distribution as simulated in FLUKA for different proton beam energies impinging on a $1-\mu$m silicon cube. Results are normalized per incident particle.

TABLE I

FRACTION OF HADRON SPECTRUM ABOVE 20 MeV WITH ENERGIES LARGER THAN A CERTAIN VALUE

Environment	Source	Fraction above		
		200 MeV	500 MeV	1 GeV
Trapped protons	CREME [9]	0.18	0.01	-
Sea-level	JEDEC [2]	0.32	0.10	0.06
12 km	QARM [10]	0.40	0.20	0.12
LHC tunnel	FLUKA [11]	0.41	0.30	0.20
Interplanetary	CREME [9]	0.93	0.76	0.55

800-km altitude, 98° orbit for solar minimum conditions, and 100 mils of aluminum shielding. The same shielding and solar conditions are used to derive the proton galactic cosmic ray (GCR) interplanetary spectrum. The relevant environment for avionics considers the sum of the neutron and proton spectra at a 12-km altitude, for a latitude of 46° N and longitude of 6° E (Geneva, Switzerland). For ground level, the JEDEC reference neutron spectrum in New York is considered. For the LHC, a FLUKA simulation was performed to determine the particle energy spectra below the cryostat of the magnets in the tunnel, where the electronics equipment is typically hosted.

As can be seen, the trapped proton belt and sea-level JEDEC neutron spectra are the two softest environments. However, as summarized in Table I, respectively, 18% and 32% of the >20-MeV flux remains above 200 MeV. For the 12-km (neutrons and protons) and LHC tunnel [7], [8] (pions, protons and neutrons) spectra, the levels are more energetic, with the latter having 30% of its spectrum above 500 MeV. Finally, the interplanetary proton spectrum is clearly the hardest of all those considered, with more than half of the flux above 20 MeV having energies larger than 1 GeV. The implications of such energy spectra on the SEE response and associated RHA will be discussed in Section VII.

III. MONTE CARLO SEE CROSS SECTION MODELING

Monte Carlo (MC) codes such as FLUKA [11], [12] can accurately model the energy deposition from nuclear fragments in a defined region corresponding to the SEE sensitive volume (SV) of a component. Such models can successfully predict the SEE cross section of particles and energies which are not accessible in standard test facilities but still relevant to the operational environment [13], [14]. Such would be the case for instance of GeV/n ions in space or pions, protons, and neutrons in the 100 MeV–10 GeV range in accelerators, just to mention a few.

Whereas in order to more accurately describe the response of a component to an energy deposition event, Monte Carlo codes typically need to be coupled with semiconductor device simulations such as technology computer-aided design we apply a simple model in which an SEE event is assumed to take place for every event depositing an energy larger than a certain critical value. This so-called rectangular parallelepiped (RPP) Monte Carlo modeling is still broadly used in the SEE calculations [15].

The main model parameters for the FLUKA simulation of the two SRAMs considered in this paper are shown in Table II. As to what concerns the critical charge, in the case of Device A, it was retrieved by finding the best fit of the simulated proton SEU cross section to the measured data in the 30–230-MeV interval [13]. It is worth noting that the value is consistent with the 8 fC referenced in [16] for the considered technology. As to Device B, the value is based on the critical charge attributed to the SRAM cell itself, plus that associated with the additional dynamic random access memory (DRAM) capacitor used to enhance the SEU resistance of the device [14].

The RPP SV dimensions were assumed to be twice the transistor drain size in the x/y surface, whereas the thickness is established according to the generally assumed charge collection depth for SEU. In addition, the back-end-of-line (BEOL) geometry and materials were defined as a simplified version of the information provided by the manufacturer or obtained through scanning electron microscope (SEM) inspection.

Despite the advantages related to the application of the simple RPP plus critical charge model introduced above to the calculation of SEE cross sections for a broad variety of particles and energies, there are still important limitations related to: 1) the simplified charge collection and response model and 2) the natural lack of accurate knowledge of the SV topology, critical charge, and detailed geometry.

The resulting simulated cross sections will be presented together with the experimental results in Section V. However, Figs. 2 and 3 already show that from a secondary particle

TABLE II

MAIN FLUKA MODEL PARAMETERS FOR THE TWO SRAMS CONSIDERED, HEREAFTER REFERRED TO, RESPECTIVELY, AS DEVICES A AND B. THE DIMENSIONS CORRESPOND TO x, y, AND z (THICKNESS)

Reference	Feature size (μm)	SV dimensions size (μm)	Q_{crit} (fC)	BEOL Materials
AT68166F	0.25	$0.6 \times 0.6 \times 0.6$	9.8	SiO_2, Al
R1LV1616R	0.15	$0.35 \times 0.45 \times 0.40$	66	SiO_2, Al, W

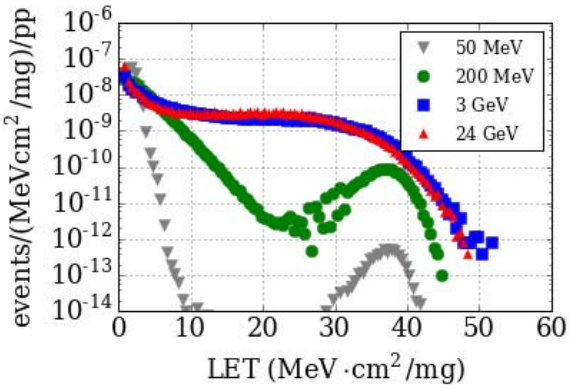

Fig. 3. Nuclear reaction product LET distribution as simulated in FLUKA for different proton beam energies impinging on a $1-\mu$m tungsten cube. Results are normalized per incident particle.

production level, whereas in the case of silicon, the LET distribution of nuclear reaction products is hardly altered between 200 MeV and 24 GeV; in the case of tungsten, there is a significant increase in the high-LET fragment production, already between 50 MeV and up to 3 GeV. The situation saturates above this energy and therefore is very similar for the case of the 24-GeV proton beam. Therefore, regardless of the energy deposition distribution, Figs. 2 and 3 already show that a much stronger energy dependence is expected for cross section driven by high-Z fragments as opposed to silicon (or similar) elements.

IV. CHARM IN-BEAM CHARACTERISTICS

The CHARM facility is typically operated through the interaction of a 24-GeV proton beam with a 50-cm metallic target generating a mixed field similar to that present in the high-energy accelerator environment [1]. However, the target can also be removed, thus allowing for the direct exposure of components and boards to the 24-GeV proton beam, as can be seen in Fig. 4. In order to obtain the required homogeneity in the center of the beam, the latter is defocused in the vertical direction through the settings of four quadrupole magnets in the T8 beam of the PS experimental EA, and swept across the horizontal direction during the 350-ms spill. The resulting beam profile is shown in Fig. 5 for the horizontal direction, as measured with a multi wire proportional chamber (MWPC). Provided the large beam size and penetrating radiation fields, a broad set of components and/or boards can be tested in parallel without altering the beam energy, shape, and intensity. However, the possible impact of the board material on the beam intensity and secondary particle production needs to be evaluated with specific Monte Carlo simulations.

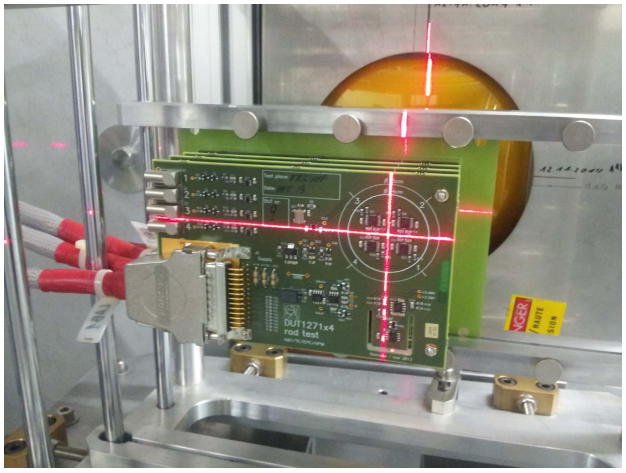

Fig. 4. Image of the ADS1271B setup in the CHARM in-beam position aligned with the laser system.

In addition, the time structure of the spill is measured through the beam position monitors [17] in the IRRAD facility upstream CHARM. In the first approximation, the beam intensity can be considered as constant over the spill, with no specific substructure due to the slow extraction from the PS synchrotron accelerator. Therefore, provided the spill time is long compared to typical SEE response times (i.e., in the ~ns range) the time structure is not expected to impact the tested component's response.

In addition, there is a dedicated mechanical support for components and boards that is automatically transported to the in-beam position together with its cabling through a rail system in order to minimize the exposure of workers to the residual dose in the internal area of the facility. The cable distance between the in-beam position and the control room is roughly 40 m. As shown in Fig. 4 , a laser alignment system is also available. Moreover, an x-y table compatible with the movable platform has recently been developed and installed.

The proton beam is pulsed with spills of roughly 350 ms occurring between one and six times of every 45 s. The beam intensity is measured with a secondary emission counter (SEC) which is regularly calibrated with aluminum activation measurements, and can be considered to have an uncertainty of 10% mainly deriving from the considered nuclear cross section for the radioactive isotope production.

The nominal spill intensity is $1-5\times10^{11}$ protons. The beam intensity can be regulated in this interval through the so-called shaving of the beam in the PS Booster—the accelerator that injects the beam in the PS at 1.4 GeV. Low intensity extractions are possible with spills of $3\times10^{8}-2\times10^{9}$ protons. This is achieved by combining the PS Booster shaving with shorter injection times from the LINAC2 (50 MeV) to the PS Booster. A summary of the resulting fluxes and dose rates can be found in Table III.

A. Beam Profile Measurements

The beam profile in the CHARM facility is measured by means of an MWPC directly downstream from the device

TABLE III

BEAM CHARACTERISTICS CONSIDERING BOTH THE LOW AND HIGH INTENSITY BEAM OPTIONS. SIX SPILLS PER 45 s CYCLE AND AN 80×100 mm^2 FWHM SIZE ARE CONSIDERED

Spill intensity	Flux (p/cm^2/s)	Dose Rate (Gy[SiO_2]/h)
$3 \times 10^9 - 2 \times 10^{10}$	$3.9 \times 10^6 - 2.6 \times 10^7$	8.4-56
$1 \times 10^{11} - 5 \times 10^{11}$	$1.3 \times 10^8 - 6.5 \times 10^8$	280-1400

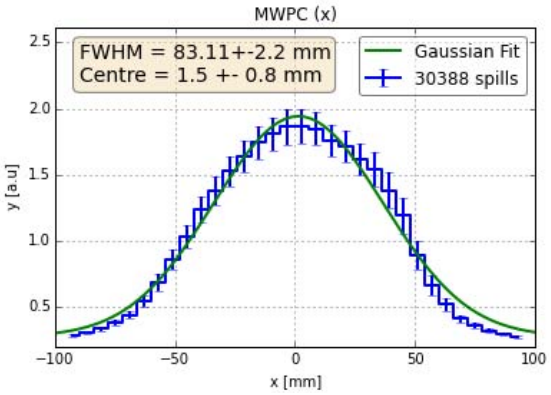

Fig. 5. Horizontal beam profile as measured with the MWPC and corresponding Gaussian fit.

under test (DUT) position. An image of the average horizontal beam profile during a run lasting several days is shown in Fig. 5, together with the respective Gaussian fit. A similar profile was obtained for the vertical direction with a full width half maximum (FWHM) of 102 mm, yielding a beam size of 83×102 mm^2 and therefore providing a very homogeneous fluence in its center for typical DUT dimensions.

In addition, the beam 2-D profile can be monitored in relative dose terms by means of a hard-drawn (HD) V2 radiochromic dosimetry film, with a quoted dynamic range of 10–1000 Gy. The scanned and digitalized dose profile can be seen in Fig. 6. The 1-D projections of the profile measured with the radiochromic film were in excellent agreement with those obtained using the MWPC. The radiochromic film is presently under calibration in a broad variety of radiation environments with the objective of using it as a means of absolute total ionizing dose (TID) measurement.

B. Fluence Measurements Through Activation

Activation measurements were performed with aluminum foils of different sizes, ranging from 1×1 to 2×2 cm^2 and covering a total size of 10×10 cm^2. For the central part of the beam, the fluence per unit beam proton retrieved through the activation measurement was 9.78×10^{-3} p/cm^2/pot, where pot stands for protons on target, and which when divided by the fluence value independently obtained from the beam intensity SEC measurement and profile, yielded a relative result of 0.98, thus fully compatible with it. The cross section used for the fluence calculation from the activation was 10.3 mb for the ^{27}Al(p,X)^{22}Na reaction at 24 GeV [18]. The half-life of the ^{22}Na isotope is 2.603 yr, with an emitted gamma ray of 1274.5 keV.

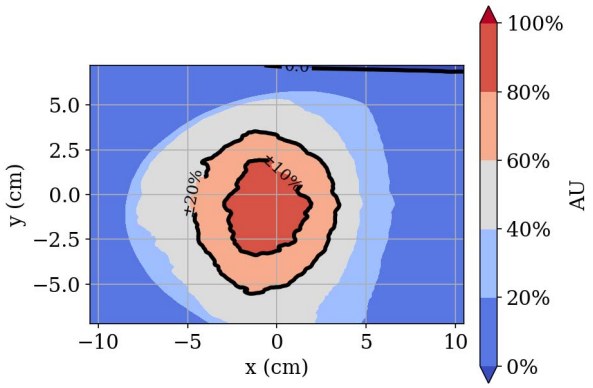

Fig. 6. 2-D dose map as retrieved using an HD V2 radiochromic film, showing the 10% and 20% homogeneity contour plots.

V. SEE CROSS SECTION MEASUREMENTS

A. Device A: ESA SEU Reference Monitor

The European Space Agency (ESA) SEU reference monitor [19], here referred to as *Device A*, is a 0.25 μm CMOS-based SRAM calibrated in a broad range of experimental conditions. In addition to providing the total number of SEUs, their physical distribution in the 2×2 cm^2 sensitive surface is displayed, thus also enabling the evaluation of the beam homogeneity.

Two different components were tested in the 24-GeV proton beam at CHARM yielding an average cross section result of 7.56×10^{-14} cm^2/bit. For the total fluence of 8.12×10^{10} p/cm^2, more than 1.03×10^5 SEUs were accumulated, homogeneously distributed over the ESA monitor sensitive surface.

This cross section value is roughly three times larger than that measured at 200 MeV, and as can be seen in Fig. 7 is in good agreement with, while visibly above, the FLUKA simulated cross section through the model introduced in Section III. It is to be noted that as predicted through simulation and measured experimentally, the increase in the SEU cross section is mainly due to the presence of a $250 - \mu$m Kovar lid on top of the active part of the memory. Light fragments are produced in the interactions between the 24-GeV proton and the lid material at a larger rate and with longer ranges at GeV energies [13]. In fact, the cross section value without the lid was fully compatible with that obtained at 200 MeV, as expected by the very similar nuclear product LET distribution shown in Fig. 2. Therefore, the ~30% discrepancy between the simulation and experimental data at 24 GeV could be partially attributed to the not fully accurate description of the lid materials and thickness.

B. Device B: Renesas SRAM

SEU and multiple bit upset tests were performed on the R1LV1616R low power 16-Mbit SRAM (date code 1328) from Renesas, referred to here as *Device B*. The part is fabricated using a 0.15-μm CMOS technology and thin-film transistor layout. The component was irradiated up to a fluence of 1.42×10^{11} p/cm^2, corresponding to 45 Gy.

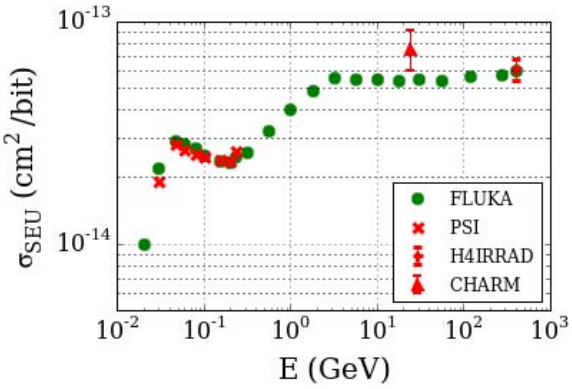

Fig. 7. Measured and simulated proton SEU cross section for Device A as a function of energy. More information about the rest of the monoenergetic data shown can be found in [13].

TABLE IV
EVENT STATISTICS FOR DEVICE B

Event	Number	Cross Section (cm^2/bit)
Total events	764	3.22×10^{-16}
SEU	842	3.53×10^{-16}
SBU	697 (91%)	2.93×10^{-16}
MBU(2)	56 (7%)	2.36×10^{-17}
MBU(3)	11 (1%)	4.63×10^{-18}
MBU(>3)	0	-

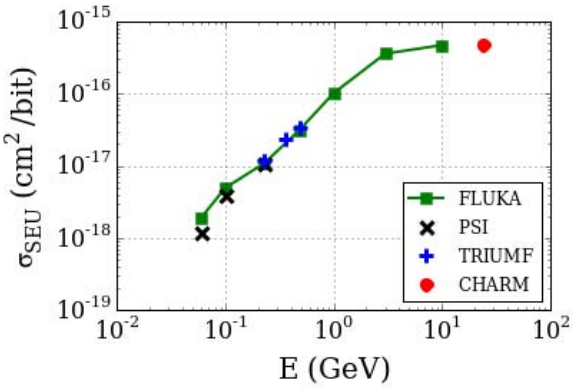

Fig. 8. Measured and simulated proton SEU cross section for Device B as a function of energy. More information about the rest of the monoenergetic data shown can be found in [14].

The associated event statistics is shown in Table IV. Therefore, the 24-GeV proton event SEU cross section corresponds to 3.22×10^{-16} cm^2/bit.

As can be seen in Fig. 8, this corresponds to an increase of roughly a factor of 30 with respect to the experimental results at PSI using the 200-MeV protons. The response is in very good agreement with the FLUKA model of the sensitive region and surrounding material introduced earlier, including a tungsten volume compatible with what was observed in the SEM analysis.

In contrast to what was shown in [20], the works in [14] and here show that the component SEU cross section is low not because of a high energy onset, but rather because of the very strong dependence of the cross section with energy due to the dominance of high-Z fission fragments.

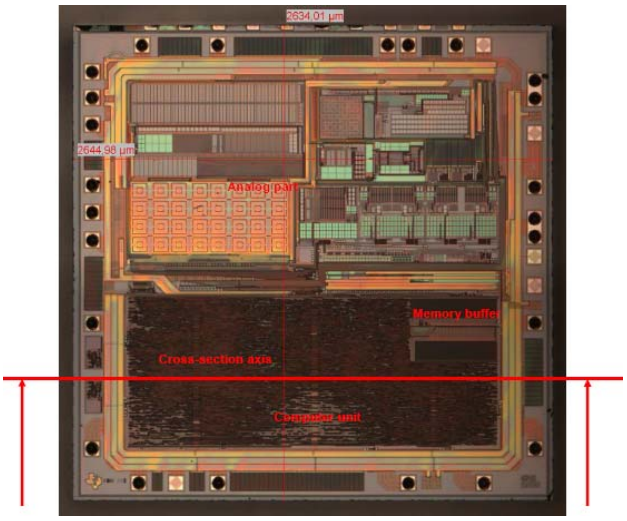

Fig. 9. De-lidded sample for heavy ion testing. The horizontal line corresponds to the cross section axis for the SEM shown in Fig. 10. The bottom area of the component is the digital part, whereas the top corresponds to the analog. The size of the chip is 2.6×2.6 mm^2.

C. Device C: ADS1271B

The ADS1271B ADC, here denoted as *Device C*, is a 24-bit, delta-sigma ADC from Texas Instruments with a data rate up to 105 kSPS. The part was selected as a candidate component for the FGClite power converter controls system at CERN to be installed in the LHC tunnel [21]. The ADC was categorized as a highly critical component in the system, being in its critical failure path.

Owing to its low sensitivity to protons and in order to enhance its error count statistics, the part was tested in a configuration enabling up to 16 individual parts to be irradiated simultaneously, through four stacked boards each containing four components, as shown in Fig. 4. An image of the open part can be seen in Fig. 9. A cross section analysis was performed through SEM as can be seen in Fig. 10. The cross section inspection through polishing and SEM was complemented with an energy dispersive X-ray spectroscopy for material analysis.

The part used a three metals plus one polysilicon process. The M1, M2, and M3 layers were made of aluminum. Transistor gates at polysilicon level were compatible with a $0.3 - \mu$m node process. The via 1 and 2 contacts were made of tungsten, as can be seen in Fig 10. The vias were roughly 1 μm thick in the vertical direction of the figure.

The parts were also tested for heavy ions at the CYCLONE facility in Université Catholique de Louvain (UCL), showing SEL sensitivity both in the analog (5 V) and digital (1.8 V) blocks. The respective cross sections, measured separately, both had saturation values of roughly 5×10^{-5} cm^2 at LET values of 40 MeV cm^2/mg and estimated LET thresholds near 10 MeV cm^2/mg. The SEL detection was carried out through the threshold currents of 25 and 20 mA, respectively, for the analog and digital parts. The hold and cut times were set to 1 and 7 ms. Heavy ion tests were carried out at 60 °C and using both the high LET ($E = 4$ MeV/n) and high penetration ($E = 10$ MeV/n) cocktails. Two different lots were

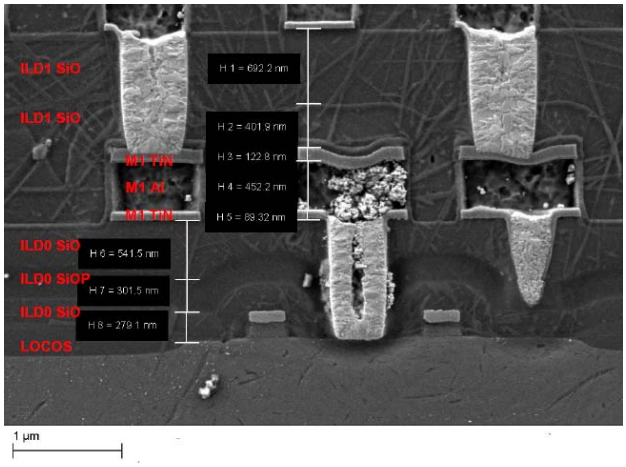

Fig. 10. SEM image of the ADS1271B ADC component (Device C), showing the tungsten presence in light gray.

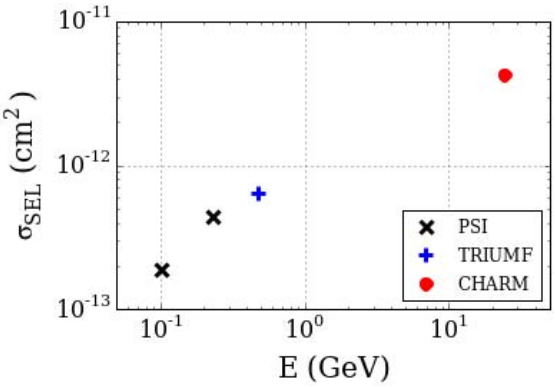

Fig. 11. Measured proton SEL cross section for Device C as a function of energy in different facilities.

TABLE V
HEAVY ION SEL CROSS SECTION FOR DEVICE C AS MEASURED IN UCL AT 60 °C AND IN MODULATOR MODE, FOR BOTH ANALOG (AVDD) AND DIGITAL (DVDD) PARTS

Ion	Energy (MeV/n)	Range (μm)	LET (MeVcm^2/mg)	σ_{SEL} (cm^2)	
				AVDD	DVDD
^{84}Kr	3.6	39	40.4	$4.21 \cdot 10^{-5}$	$6.44 \cdot 10^{-5}$
^{58}Ni	9.8	100	20.4	$1.24 \cdot 10^{-5}$	$2.21 \cdot 10^{-5}$
^{40}Ar	9.3	117	10.2	$4.00 \cdot 10^{-7}$	$2.50 \cdot 10^{-7}$
^{22}Ne	10.7	216	3	$< 1.80 \cdot 10^{-7}$	$< 1.80 \cdot 10^{-7}$

tested. The largest hold current reached was 450 mA, and was reached in the analog part. On the digital part, the maximum value was 65 mA. The SEL tests were carried out in modulator mode. The respective cross section values for the digital and analog part are shown in Table V.

SEL proton tests were performed at PSI (100 and 230 MeV), TRIUMF (480 MeV), and CHARM (24 GeV). The resulting proton cross section as a function of energy can be seen in Fig. 11. As can be seen, the cross section increased by over a factor of 40 between 100 MeV and 24 GeV. The respective SEL rate was evaluated through the convolution of the cross section and the particle energy spectra in the high energy accelerator, and was deemed to be too large for a component categorized as critical. If the 100- or 200- MeV cross sections had been taken as the saturation value, the SEL probability would have been low enough to accept the part's selection, potentially leading to a larger than expected operational SEL rate due to the harder spectra in operation.

VI. IMPACT OF HIGH-Z MATERIALS IN A GENERIC SEE MODEL

In [5], the impact of high-Z materials on SEL cross sections was first studied, suggesting that tests should be carried out at the maximum temperature and proton energy of the system environment. Alternatively, heavy ion beams of an LET of >40 MeV cm^2/mg could be used to ensure that devices are SEL-free in a proton environment.

In [22], it was shown that an operational amplifier with an LET threshold in the 16–20 MeV cm^2/mg range depending on the supply voltage suffered destructive single event dielectric rupture with a 200-MeV proton beam only in the presence of its gold plated lid. In the analysis, the importance of testing at the maximum proton environment energy is stressed in the context of the trapped proton belt due to the strong fission cross section energy dependence above energies typically used in the ground level SEE testing (i.e., 200 MeV). This is particularly important for relatively light high-Z materials such as tungsten, for which the saturation energy is above 1 GeV. Other heavier materials such as gold have lower saturation energies; therefore the constraint on the maximum experimental energy is more relaxed. An analysis expanded to other fissile materials and package topologies is available in [23].

The impact of high-Z materials on the equivalent LET produced by protons has also been investigated in the context of evaluating proton testing as a means of screening the heavy ion sensitivity [4], [24], [25]. In this context, the equivalent LET is defined as the deposited energy (typically through indirect energy deposition in the case of protons) divided by the SV thickness. The main conclusion is that even if at high energies (>200 MeV) and proton fluences ($>10^{12}$ cm^{-2}) the presence of tungsten will result in an increased equivalent LET production, this can hardly be exploited for correlating the proton SEE rate with that in a heavy ion environment due to the lack of knowledge of the high-Z material species, quantity, and location.

Whereas testing at the worst case, maximum energy present in the trapped proton environment ($\sim$500 MeV) is feasible at cyclotron test facilities such as TRIUMF [26], for harder spectra such as the atmospheric or high-energy accelerator environments (see Fig. 1) this is clearly not the case. Therefore, as detailed in [27]–[29], for such hard environments it is recommended to either test in spallation sources representative of the spectral hardness, or apply safety margins on the cyclotron data according to calculation results for a pessimistic high-Z material presence and the corresponding operational environment.

Provided we will, in addition, be analyzing the impact of proton induced nuclear fragments in an environment typically dominated by heavy ion direct energy deposition such as that

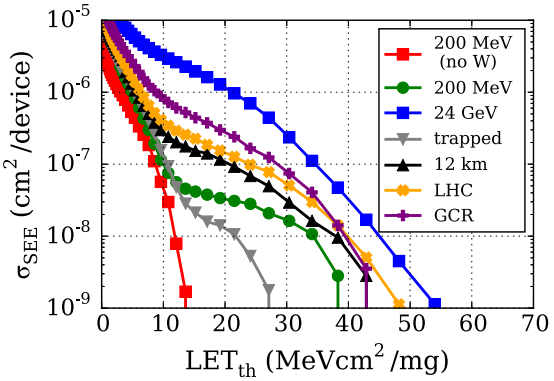

Fig. 12. Simulated SEE cross section as a function of threshold LET for different environments and the generic RPP model described in the text with a $1-\mu$m tungsten slab directly above the SV.

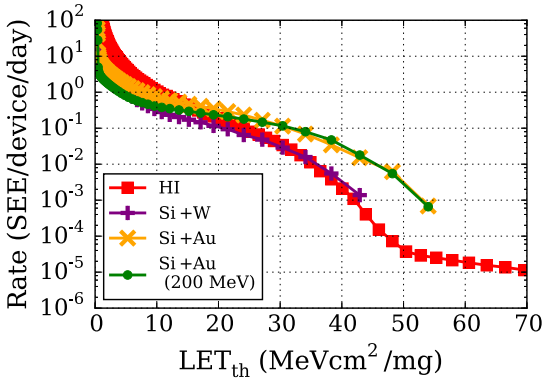

Fig. 13. Simulated SEE rate as a function of threshold LET for different environments and the generic RPP model described in the text with a $1-\mu$m tungsten and $5-\mu$m gold slabs directly above the SV.

of GCRs, it is important to consider the possible contribution from heavy ion nuclear reactions.

As initially shown in [30], low-LET cross section measurements for high-LET threshold components were attributed to nuclear interactions from the heavy ion beam with the device's materials, as opposed to specific highly sensitive regions of the circuit. As in the case of protons, the probability of high-LET secondaries from ion reactions is strongly dependent on the material, and can be particularly SEE threatening for high-Z materials such as tungsten. In [31], it was shown that for the sub-LET threshold area and for a given LET value, the SEE cross section strongly increases with the ion energy in the 1–40 MeV/n range, suggesting that ground level testing, typically carried out at around 10 MeV/n, could significantly underestimate the in-flight indirect heavy ion SEE rate owing to the larger GCR energies, peaking at ~1 GeV/n.

In [32], it was shown through a combination of the ground test and in-flight data with Monte Carlo simulations that in some cases (e.g., high LET threshold and high-Z materials near the sensitive regions) the contribution of reaction products to the event rate in the space radiation environment can dominate the overall response. These results are supported by the work in [33] that shows through direct charge collection measurements and associated simulations that for critical charges larger than those deposited by direct ionization, the nuclear reactions, and therefore, beam energy, species, and involved device materials will strongly affect the energy deposition distribution, and the SEE cross sections.

However, whereas the experimental and simulated data in [31] and [33] used heavier ions for larger energies in order to reproduce the same LET, more recent test and calculation results in [34] and [35] show that for a given ion, the sub-LET threshold SEE cross section in fact decreases in the 10–100 MeV/n range owing to the decreased contribution from complete and break-up fusion of the projectile ion and target nucleus. In addition, [35] shows that the nuclear reaction SEE rate for a GCR environment is expected to be dominated by protons owing to their much larger fluences and relatively similar (within a factor ~3 of heavy ions) sub-LET SEE cross section at larger energies.

It is clear from the above-mentioned discussion that the representativeness of an experimental environment for a given component and operational scenario will depend on: 1) the respective monoenergetic test beam and operational radiation environment; 2) the materials surrounding the sensitive regions; and 3) the device's SEE response as a function of deposited energy. The simulations for the SRAMs shown in Section V are specific to a certain tungsten amount and distribution, as well as to a given heavy ion response and/or critical charge assumption. Therefore, in order to extract more general RHA implications, we will consider a simple model, consisting of a $10-\mu$m side cube silicon target with a $1-\mu$m side cube SV in the center, and a $1-\mu$m thick tungsten slab immediately above it. This amount of tungsten would typically be large with respect to standard metallization and plugs found in typical ICs (See Fig. 10 or the SRAMs analyzed through SEM in [14] and [29]); however, it serves the purpose of describing a response dominated by a high-Z material.

This model is implemented in FLUKA and the environments described in Section II are used as sources in the simulation. The respective SEE cross sections as a function of critical equivalent LET are extracted assuming a total device sensitive surface of 1 cm^2. In addition to the environmental cases, the monoenergetic beams of 200 MeV and 24 GeV are also included. For the cases with multiple particles and energies, the cross section is defined based on the fluence of hadrons above 20 MeV. For the space environment, an isotropic, solar minimum flux extracted from CREME96 [9], [36] and 100 mils of aluminum shielding are considered, whereas for the rest of cases we assume a monodirectional beam normal to the component's surface. The resulting SEE cross sections as a function of threshold equivalent LET for the different environments can be seen in Fig. 12. The main advantage of plotting the results in terms of cross sections and as a function of the threshold equivalent LET is that different environments and geometries (e.g., with versus without tungsten slab) can be directly compared. The implications of such calculated SEE cross sections will be covered in Section VII.

As opposed to the atmospheric, LHC, and (to a certain extent) trapped proton environments, in the case of the interplanetary environment, in addition to the proton GCR spectrum, other heavier ion species will be present that will typically dominate the overall SEE rate through direct

ionization. In order to compare the relative impact of direct and indirect energy deposition from proton-induced high-Z material fission, the direct ionization SEE rate is plotted in Fig. 13 as extracted with CREME MC [37], [38] for an interplanetary environment with ions up to $Z = 92$ (uranium) and a $1 - \mu m^3$ silicon SV; together with that obtained from FLUKA using the proton GCR environment as an input and the SEE model introduced earlier. In addition to the $1 - \mu m$ tungsten case, a $5 - \mu m$ gold case is also considered in order to mimic the gold-plated package studied in [22]. For the gold plated case, the respective SEE rate as extracted from 200-MeV proton measurements is also included as obtained by multiplying the cross section times the proton flux above 20 MeV. The implications of such calculated cross sections will be covered in Section VII.

VII. Radiation Hardness Assurance Implications

As can be seen in Fig. 12, in the case of tungsten-dominated cross sections (i.e., significant high-Z material presence near the SV and an LET threshold above ~15 MeVcm^2/mg), testing up to 200-MeV proton energies is sufficient to reproduce the effect of the trapped proton belts; however, this is clearly not the case for the other three, harder environments: GCR protons, atmospheric neutrons and protons at a 12-km altitude, and hadrons in the LHC tunnel. The underestimation of the SEE rate when applying 200-MeV cross sections to such environments in the tungsten-dominated case when considering an LET threshold of 20 MeVcm^2/mg is, respectively, 8.8, 3.4, and 4.6. Such values are fairly constant with the LET threshold as can be seen in Fig. 12. Therefore, if tested at 200 MeV, such factors would need to be applied as safety margins for the operation in the respective environments in order to account for the possible impact of the increased SEE risk at larger energies.

For all cases, however, the 24-GeV proton beam represents a worst case SEE cross section scenario, and will yield values a factor ~40 larger than for 200 MeV for tungsten-dominated cross sections. This can be advantageous both in terms of obtaining an upper bound to the operational SEE rate, and in reaching a given number of events in a much shorter time or with a much lower TID level than at 200 MeV. This practical advantage is particularly relevant when the need exists of qualifying components down to very small SEE cross section values due to the large number of parts involved in operation, such as for LHC distributed systems [39].

In the case of heavier high-Z materials such as gold or lead, the saturation fission cross section is reached at lower energies, as also shown in [22] and [40]. Therefore, 200-MeV protons are energetic enough to reproduce the SEE effects at larger energies even for the highly energetic environments mentioned earlier. This is clearly shown in Fig. 13, which also reflects that above an LET threshold of roughly 20 MeVcm^2/mg, 5 μm of gold directly above the SV are capable of dominating the overall SEE rate with respect to heavy ion direct ionization, and this by more than two orders of magnitude for an LET threshold of roughly 50 MeVcm^2/mg. In the case of tungsten, however, with a smaller considered thickness (1 μm as opposed to 5 μm) and a lower associated fission cross section, the indirect energy deposition is not dominant and is only comparable to the direct energy deposition above roughly 30 MeVcm^2/mg.

VIII. Summary and Conclusion

We present the 24-GeV proton beam at CHARM, of a size of roughly 80×100 mm^2 FWHM and the flux and dose rate levels shown in Table III. The beam properties are monitored with a calibrated SEC for the intensity and an MWPC for the profile. The measured intensities and beam profiles are in excellent agreement with those obtained using other techniques such as activation, RadFETs, [41] or radiochromatic films.

The beam can be used to test multiple components and boards at an energy which almost fully covers the energy spectra for a wide variety of applications, including the LHC tunnel hadron and interplanetary proton environments. Examples of two SEU and an SEL response are shown for components with cross sections dominated by silicon in one case and tungsten in the other two. The very different energy dependence is discussed with the aid of Monte Carlo models, in very good agreement with the experimental data. It is shown that for components with SEE cross sections dominated by high-Z fragments, the dependence of the response with energy up to roughly 3 GeV is significant. Therefore, qualifying at standard proton cyclotron facilities might lead to an underestimation of the application failure rate for highly energetic environments.

In particular, the RHA implications of such SEE cross section energy dependence are explored through generic SEE models. Whereas the quantitative implications derived from them strongly depend on the amount and distribution of the high-Z material with respect to the SV, the results can be used to qualitatively establish that: 1) whereas for SEEs driven by tungsten-like fission fragments, typical proton cyclotron energies (i.e., 200 MeV) can lead to a significant underestimation of the operational SEE rate for harder environments such as GCR protons, 12-km atmospheric or the LHC tunnel; the 24 GeV presented here represents worst case testing conditions and 2) for gold-like dominated cross sections, 200-MeV protons are sufficient to reproduce the SEE probability at larger energies. In addition, for a GCR environment, the indirect energy deposition from proton-induced gold fission fragments can potentially dominate the overall SEE rate for high (>20 MeVcm^2/mg) LET threshold values.

In addition to the proton beam, highly energetic heavy ions beams are planned at CHARM in the near future. The main applications for such beams (Xe or Pb of an energy of ~6 GeV/n) is that of allowing for the qualification of complex components for which the sensitive region is not easily accessible through the standard ion tests at energies of ~10 MeV/n and corresponding to ranges in silicon between 200 μm (light ion, N) and 90 μm (heavy ion, Xe). In addition, the analysis of the impact of the beam energy on aspects such as the nuclear induced SEE [34] or ion track structure [42], [43] is also a key motivation for developing and exploiting such a high-energy ion beam.

REFERENCES

[1] J. Mekki, M. Brugger, R. G. Alía, A. Thornton, N. C. D. S. Mota, and S. Danzeca, "CHARM: A mixed field facility at CERN for radiation tests in ground, atmospheric, space and accelerator representative environments," *IEEE Trans. Nucl. Sci.*, vol. 63, no. 4, pp. 2106–2114, Aug. 2016.

[2] *Measurement and Reporting of Alpha Particle and Terrestrial Cosmic Ray-Induced Soft Errors in Semiconductor Devices*, JEDEC Standard JESD89A, 2006.

[3] D. M. Hiemstra and E. W. Blackmore, "LET spectra of proton energy levels from 50 to 500 MeV and their effectiveness for single event effects characterization of microelectronics," *IEEE Trans. Nucl. Sci.*, vol. 50, no. 6, pp. 2245–2250, Dec. 2003.

[4] R. Ladbury, J.-M. Lauenstein, and K. P. Hayes, "Use of proton SEE data as a proxy for bounding heavy-ion SEE susceptibility," *IEEE Trans. Nucl. Sci.*, vol. 62, no. 6, pp. 2505–2510, Dec. 2015.

[5] J. R. Schwank *et al.*, "Effects of particle energy on proton-induced single-event latchup," *IEEE Trans. Nucl. Sci.*, vol. 52, no. 6, pp. 2622–2629, Dec. 2005.

[6] H. H. K. Tang, "Nuclear physics of cosmic ray interaction with semiconductor materials: Particle-induced soft errors from a physicist's perspective," *IBM J. Res. Develop.*, vol. 40, pp. 91–108, Jan. 1996.

[7] K. Roeed *et al.*, "Method for measuring mixed field radiation levels relevant for SEEs at the LHC," *IEEE Trans. Nucl. Sci.*, vol. 59, no. 4, pp. 1040–1047, Aug. 2012.

[8] R. G. Alía *et al.*, "LHC and HL-LHC: Present and future radiation environment in the high-luminosity collision points and RHA implications," *IEEE Trans. Nucl. Sci.*, vol. 65, no. 1, pp. 448–456, Jan. 2018.

[9] A. J. Tylka *et al.*, "CREME96: A revision of the cosmic ray effects on micro-electronics code," *IEEE Trans. Nucl. Sci.*, vol. 44, no. 6, pp. 2150–2160, Dec. 1997.

[10] F. Lei, S. Clucas, C. Dyer, and P. Truscott, "An atmospheric radiation model based on response matrices generated by detailed Monte Carlo simulations of cosmic ray interactions," *IEEE Trans. Nucl. Sci.*, vol. 51, no. 6, pp. 3442–3451, Dec. 2004.

[11] G. Battistoni *et al.*, "Overview of the FLUKA code," *Ann. Nucl. Energy*, vol. 82, pp. 10–18, Aug. 2015.

[12] T. Böhlen *et al.*, "The FLUKA code: Developments and challenges for high energy and medical applications," *Nucl. Data Sheets*, vol. 120, pp. 211–214, Jun. 2014.

[13] R. G. Alía *et al.*, "SEE measurements and simulations using monoenergetic GeV-energy hadron beams," *IEEE Trans. Nucl. Sci.*, vol. 60, no. 6, pp. 4142–4149, Dec. 2013.

[14] S. Uznanski *et al.*, "The effect of proton energy on SEU cross section of a 16 Mbit TFT PMOS SRAM with DRAM capacitors," *IEEE Trans. Nucl. Sci.*, vol. 61, no. 6, pp. 3074–3079, Dec. 2014.

[15] R. A. Reed *et al.*, "Physical processes and applications of the Monte Carlo radiative energy deposition (MRED) code," *IEEE Trans. Nucl. Sci.*, vol. 62, no. 4, pp. 1441–1461, Aug. 2015.

[16] P. Roche, G. Gasiot, K. Forbes, V. O'Sullivan, and V. Ferlet, "Comparisons of soft error rate for SRAMs in commercial SOI and bulk below the 130-nm technology node," *IEEE Trans. Nucl. Sci.*, vol. 50, no. 6, pp. 2046–2054, Dec. 2003.

[17] F. Ravotti *et al.*, "The beam profile monitoring system for the CERN IRRAD proton facility," in *Proc. Int. Beam Instrum. Conf.*, Oct. 2016, pp. 1–5. [Online]. Available: https://cds.cern.ch/record/2235850

[18] G. L. Morgan *et al.*, "Total cross sections for the production of ^{22}Na and ^{24}Na in proton-induced reactions on ^{27}Al from 0.40 to 22.4 GeV," *Nucl. Instrum. Methods Phys. Res. B, Beam Interact. Mater. At.*, vol. 211, pp. 297–304, Nov. 2003.

[19] R. Harboe-Sorensen *et al.*, "The technology demonstration module onboard PROBA-II," *IEEE Trans. Nucl. Sci.*, vol. 58, no. 3, pp. 1001–1007, Jun. 2011.

[20] R. Velazco *et al.*, "Evidence of the robustness of a COTS soft-error free SRAM to neutron radiation," *IEEE Trans. Nucl. Sci.*, vol. 61, no. 6, pp. 3103–3108, Dec. 2014.

[21] S. Uznanski, B. Todd, A. Dinius, Q. King, and M. Brugger, "Radiation hardness assurance methodology of radiation tolerant power converter controls for large hadron collider," *IEEE Trans. Nucl. Sci.*, vol. 61, no. 6, pp. 3694–3700, Dec. 2014.

[22] T. L. Turflinger *et al.*, "RHA implications of proton on gold-plated package structures in SEE evaluations," *IEEE Trans. Nucl. Sci.*, vol. 62, no. 6, pp. 2468–2475, Dec. 2015.

[23] T. L. Turflinger *et al.*, "Proton on metal fission environments in an IC package: An RHA evaluation method," *IEEE Trans. Nucl. Sci.*, vol. 64, no. 1, pp. 309–316, Jan. 2017.

[24] R. L. Ladbury and J.-M. Lauenstein, "Evaluating constraints on heavy-ion SEE susceptibility imposed by proton SEE testing and other mixed environments," *IEEE Trans. Nucl. Sci.*, vol. 64, no. 1, pp. 301–308, Jan. 2017.

[25] R. G. Alía *et al.*, "Simplified SEE sensitivity screening for COTS components in space," *IEEE Trans. Nucl. Sci.*, vol. 64, no. 2, pp. 882–890, Feb. 2017.

[26] E. W. Blackmore and M. Trinczek, "Intensity upgrade to the TRIUMF 500 MeV large-area neutron beam," in *Proc. IEEE Radiat. Effects Data Workshop (REDW)*, Jul. 2014, pp. 1–5.

[27] R. G. Alía *et al.*, "SEL cross section energy dependence impact on the high energy accelerator failure rate," *IEEE Trans. Nucl. Sci.*, vol. 61, no. 6, pp. 2936–2944, Dec. 2014.

[28] R. G. Alía *et al.*, "Energy dependence of tungsten-dominated SEL cross sections," *IEEE Trans. Nucl. Sci.*, vol. 61, no. 5, pp. 2718–2726, May 2014.

[29] R. G. Alía *et al.*, "SEL hardness assurance in a mixed radiation field," *IEEE Trans. Nucl. Sci.*, vol. 62, no. 6, pp. 2555–2562, Dec. 2015.

[30] K. M. Warren *et al.*, "The contribution of nuclear reactions to heavy ion single event upset cross-section measurements in a high-density SEU hardened SRAM," *IEEE Trans. Nucl. Sci.*, vol. 52, no. 6, pp. 2125–2131, Dec. 2005.

[31] P. E. Dodd *et al.*, "Impact of heavy ion energy and nuclear interactions on single-event upset and latchup in integrated circuits," *IEEE Trans. Nucl. Sci.*, vol. 54, no. 6, pp. 2303–2311, Dec. 2007.

[32] R. A. Reed *et al.*, "Impact of ion energy and species on single event effects analysis," *IEEE Trans. Nucl. Sci.*, vol. 54, no. 6, pp. 2312–2321, Dec. 2007.

[33] N. A. Dodds *et al.*, "Charge generation by secondary particles from nuclear reactions in BEOL materials," *IEEE Trans. Nucl. Sci.*, vol. 56, no. 6, pp. 3172–3179, Dec. 2009.

[34] R. G. Alía *et al.*, "Sub-LET threshold SEE cross section dependency with ion energy," *IEEE Trans. Nucl. Sci.*, vol. 62, no. 6, pp. 2797–2806, May 2015.

[35] R. G. Alía *et al.*, "Proton dominance of sub-LET threshold GCR SEE rate," *IEEE Trans. Nucl. Sci.*, vol. 64, no. 1, pp. 388–397, Jan. 2017.

[36] Vanderbilt University, School of Engineering. *CREME Site*. Accessed: Mar. 2017. [Online]. Available: https://creme.isde.vanderbilt.edu/

[37] R. A. Weller *et al.*, "Monte Carlo simulation of single event effects," *IEEE Trans. Nucl. Sci.*, vol. 57, no. 4, pp. 1726–1746, Aug. 2010.

[38] M. H. Mendenhall and R. A. Weller, "A probability-conserving cross-section biasing mechanism for variance reduction in Monte Carlo particle transport calculations," *Nucl. Instrum. Methods Phys. Res. A, Accel. Spectrom. Detect. Assoc. Equip.*, vol. 667, pp. 38–43, Mar. 2012. [Online]. Available: http://www.sciencedirect.com/science/article/pii/S0168900211021541

[39] R. G. Alía *et al.*, "Single event effects in high-energy accelerators," *Semicond. Sci. Technol.*, vol. 32, no. 3, p. 034003, Feb. 2017. [Online]. Available: http://stacks.iop.org/0268-1242/32/i=3/a=034003

[40] R. G. Alía, "Radiation fields in high energy accelerators and their impact on single event effects," Ph.D. dissertation, Inst. d'Electron. du Sud, Univ. Montpellier, Montpellier, France, Dec. 2013, vol. 2. [Online]. Available: http://cds.cern.ch/record/2012360

[41] G. Spiezia *et al.*, "A new RadMon version for the LHC and its injection lines," *IEEE Trans. Nucl. Sci.*, vol. 61, no. 6, pp. 3424–3431, Dec. 2014.

[42] M. Bagatin, S. Gerardin, A. Paccagnella, and V. Ferlet-Cavrois, "Single and multiple cell upsets in 25-nm NAND flash memories," *IEEE Trans. Nucl. Sci.*, vol. 60, no. 4, pp. 2675–2681, Aug. 2013.

[43] G. Hubert, P. L. Cavoli, C. Federico, L. Artola, and J. Busto, "Effect of the radial ionization profile of proton on SEU sensitivity of nanoscale SRAMs," *IEEE Trans. Plasma Sci.*, vol. 62, no. 6, pp. 2837–2845, Dec. 2015.